Lawrence Berkeley National Laboratory
LBL Publications

Title

Asymmetric gas diffusion layers for improved water management in PGM-free electrodes

Permalink

https://escholarship.org/uc/item/6ck497zr

Journal

Heliyon, 10(18)

ISSN

1879-4378

Authors

Arman, Tanvir Alam

Babu, Siddharth Komini

Sabharwal, Mayank

et al.

Publication Date

2024-09-01

DOI

10.1016/j.heliyon.2024.e37222

Copyright Information

Peer reviewed

Research article

Asymmetric gas diffusion layers for improved water management in PGM-free electrodes

Tanvir Alam Arman [a,b], Siddharth Komini Babu [a], Mayank Sabharwal [c], Adam Z. Weber [c], Ugur Pasaogullari [b], Jacob S. Spendelow [a,*]

[a] Los Alamos National Laboratory, Los Alamos, NM, 87544, USA
[b] Department of Mechanical Engineering and Center for Clean Energy Engineering, University of Connecticut, Storrs, Connecticut, 06269, USA
[c] Lawrence Berkeley National Laboratory, 1 Cyclotron Rd, Berkeley, CA, 94720, USA

A B S T R A C T

Proton-exchange-membrane fuel cells (PEMFCs) offer a long-term, carbon-emission free solution to the energy needs of the transportation sector. However, high cost continues to limit PEMFC commercialization. Replacing expensive platinum group metal (PGM) catalysts with PGM-free catalysts could reduce cost, but the low active site density of PGM-free catalysts necessitates the use of thick electrodes that suffer from substantial mass transport losses. In these thick PGM-free electrodes, effective water management and oxygen transport are crucial to achieve high performance. In this work, we investigate the role of anode and cathode gas diffusion layer (GDL) configurations in controlling water management. Asymmetric GDL configurations, in which the anode GDL exhibits higher permeability than the cathode GDL, showed higher performance compared to conventional symmetric configurations. Computational modeling showed that the improved performance is mainly due to improved water management, resulting in lower liquid water saturation and faster oxygen transport in the cathode.

1. Introduction

Proton exchange membrane fuel cells (PEMFCs) are an emerging technology that can help decarbonize the transportation sector. With high energy density and power density, short refueling time, long range, and emission-free operation, PEMFCs have already shown promise in the automotive industry. However, the high cost of PEMFCs is a barrier to widespread commercialization. Cost estimates at high volume production indicate that platinum group metal (PGM) based catalysts account for about 40 % of the PEMFCs stack cost [1]. Hence, substantial research is in progress to reduce the cost by reducing the amount of PGM catalyst used or replacing the PGM-based catalyst with a low-cost PGM-free catalyst synthesized from earth-abundant transition metals (e.g., Fe, Co, Mn).

In recent years, significant improvement in kinetic activity of PGM-free catalysts [2–5] has led to achieving the DOE kinetic target for PGM-free catalysts [6,7]. With continuous efforts, PGM-free catalysts are advancing rapidly and could ultimately provide oxygen reduction reaction (ORR) performance similar to that of Pt/C catalysts, which would make them a low-cost alternative for fuel cell applications [6–12]. Despite significant improvement in kinetics, the low active site density of PGM-free catalysts necessitates the use of high catalyst loadings, resulting in thick electrodes (>100 μm) [13]. As a result, PGM-free electrodes suffer from severe mass transport losses. Hence, minimizing these transport losses is crucial step on the path to widespread adoption of PGM-free catalyst. One of the major mass transport resistances in these thick electrodes is due to the slow oxygen transport. The high thickness and low active site density of PGM-free catalyst layers (CLs) make them prone to flooding, which significantly impedes oxygen transport to active sites. Hence, improved water management is needed to avoid flooding and enhance oxygen transport [14].

A detailed understanding of oxygen and water transport phenomena is required to enable significant improvements in PGM-free fuel cell performance. The morphology of the PGM-free catalyst layer and GDL has a substantial impact on the mass transport mechanism. Among the electrode characteristics, ionomer loading, ionomer equivalent weight, catalyst layer porosity, catalyst particle size, shape, and mass loading are critical to mass transport [15–20]. GDL substrate and MPL properties also have a significant impact on oxygen and water transport. GDLs containing MPLs are used to evenly distribute the reactants from the flow field to the electrode, transport water (in both liquid and vapor phases), provide an electron conduction pathway, and provide effective contact with the catalyst layer. The GDL substrate is typically ∼200 μm thick carbon fiber paper or carbon felt with a wide range of pore sizes [21,22]. The MPL is typically around 30–50 μm thick, comprising carbon nanoparticles and fluoropolymer binder, and less porous compared to the GDL substrate [23]. In conventional GDLs, both the substrate and the MPL are typically wetproofed using fluoropolymers.

Water management in PEMFCs is a complex phenomenon. As water is generated in the cathode, effective water removal is needed to avoid flooding and maintain open pathways for oxygen diffusion. Tailoring the properties of both GDLs and MPLs can enhance water management, providing balanced water saturation for ionomer hydration while still maintaining effective oxygen transport. Different types of GDLs and MPLs having different physical and chemical properties are now commercially available from OEMs such as SGL Carbon, Freudenberg, etc. Based on the operating condition (dry or wet), and MEA fabrication method (CCM or GDE), different kinds of GDLs and MPLs are suitable [21–28]. For example, in dry conditions, GDLs with low porosity are advantageous because they retain more water and keep the membrane hydrated [27]. Introduction of hydrophilic agents or hydrophilization of the GDL has also been shown to increase membrane hydration in dry conditions [14,25,26]. At higher humidity, the use of carbon nanotubes (CNTs) in MPLs has been shown to be effective to provide preferential transport pathways for water and oxygen [29,30]. GDLs can also be physically modified to have slits or perforations that provide low capillary pressure pathways for liquid water transport [25,31]. Physical modifications of GDLs have some drawbacks, such as increased HFR due to decreased contact area between the catalyst layer and GDLs, change of optimized properties of commercial GDLs due to the fabrication process, durability issues associated with crack formation in the MEA due to strain at the edges of slits or perforations, and extra costs related to the process. Considering consistency, durability, availability, and cost effectiveness of commercial GDLs, in this study, we report a passive approach that utilizes commercial GDLs with different permeability in the anode and cathode for better water management in thick PGM-free electrodes. A 2D, steady state, multiphase, and multiphysics model was also used to study the behavior of PEMFCs with different asymmetric GDL configurations. Both experimental and modeling data showed that, for cells with a low permeability GDL in the cathode, cell performance improved as anode GDL permeability increased. This enhanced performance is due to lower liquid saturation and improved transport in the cathode. In contrast, when a highly permeable GDL was used for the cathode, the effect of anode GDL permeability was found to be minimal.

2. Experimental methods

2.1. Materials

Nafion™ 211 (Ion Power, Delaware, USA) membrane was used for all MEAs. Commercially available PGM-free catalyst (PMF 0011904 lot 1220, Pajarito Powder LLC, New Mexico, USA) and 20 wt% Pt/C (TEC10V20E, TKK, Japan) was used for the cathode and anode, respectively. Nafion™ D2020 (Ion Power, Delaware, USA) and Aquivion® D72-25BS (Sigma-Aldrich) ionomers were used in the anode and cathode, respectively. PTFE gaskets were chosen to control the compression of the GDLs. Freudenberg GDLs used in this study are listed in Table 1. As the primary goal of this work was to study water management due to the permeability change of GDLs, we chose the GDLs in such a way that parameters other than the Gurley number had minimal variation. The Gurley number represents the time it takes for a given volume of air to flow through a porous medium under a given pressure. The Gurley number listed in the Freudenberg specification data sheet is based on the ISO 5636-5 standard, which is a method used to determine the permeability. This test measures the time required for a specific volume of air to pass through a known area of a porous medium under a specific pressure differential. The most permeable GDL used was H15C14, which has a Gurley number of 0.6 s, compared to 70 s for the least permeable GDL, H14C10. All GDLs included similar substrates but different MPLs. Top view scanning electron microscopy (SEM) images of the MPL morphologies are shown in Fig. S1, while cross-sections of the GDLs are shown in Fig. S2. It is crucial to understand that the Gurley number, a measure of gas permeability, does not provide direct insights about liquid transport or diffusion transport properties. The methodology behind the Gurley number is based on convective gas flow and is significantly influenced by the pore size distribution, while liquid transport depends on factors like contact angle, and diffusion transport depends on porosity and tortuosity. In fuel cells, all these transport mechanisms occur simultaneously. While the Gurley number primarily indicates convective transport through a porous medium, it can also provide some insight into diffusion processes, though indirectly, as lower Gurley numbers (higher

Table 1
Properties of GDLs used in this study [32,33].

GDLs	Gurley number (s)	Thickness (μm)	Area weight (g/m^2)	Through plane area-specific electrical resistance(mΩ-cm^2)
H15C14	0.6	191	91	7.3
H14Cx653	15	185	94	6
H14C9	30	180	100	7
H14C7	50	175	100	6
H14C10	70	170	97	5

permeability) correspond to larger pore sizes, lower tortuosity, and higher porosity, all of which can facilitate enhanced diffusion. Therefore, the Gurley number should be considered as an indicator of relative permeability differences between the GDLs used in this study, but it does not fully capture the complexities of multiphase transport phenomena in fuel cells. Contact angle measurements showed little variation between the different GDLs (Fig. S2f), with an average angle of 140° (ranging from 131° to 144°). This suggests that the differences in Gurley number had a larger impact than the differences in contact angle in explaining the observed performance differences between the GDL configurations investigated.

2.2. MEA fabrication

Cathode catalyst inks were prepared with a solvent-to-ionomer mass ratio of 60. The solvent mixture was prepared with a 1:1 mass ratio of isopropanol and deionized water (18.2 mΩ cm). The required amount of Aquivion® D72-25BS was added to yield an ionomer to carbon ratio of 0.6. The ink was sonicated for 2 h in a bath sonicator while the temperature was maintained below 30 °C. Anode catalyst inks were prepared using nPA/water mixtures (4:3 by volume) as a solvent. The required amount of Nafion™ D2020 was added to yield an ionomer to carbon ratio of 0.5.

The MEA was fabricated with two separate ultrasonic spray coaters (Sono-TEK, Milton, NY) to avoid Pt contamination on the cathode. First, PGM-free catalyst was sprayed on one side of the membrane. The loading was measured by weighing the MEA before and after coating. The MEA was dried at 100 °C for 30 min before weighing. The loading of PGM-free catalyst was 6 ± 0.5 mg cm^{-2}. After finishing the cathode fabrication, the anode was sprayed at a loading of 0.1 mg cm^{-2} Pt, confirmed by X-ray fluorescence spectroscopy.

We tested 8 GDL configurations in this study, which were organized into two groups (Table 2). The first group included four configurations in which the cathode was fixed with the lowest permeability GDL while the anode GDL permeability was varied. The second group included four configurations in which the cathode GDL was fixed with the highest permeability GDL while the anode GDL was varied.

2.3. Cell assembly and testing

A commercially available fuel cell hardware (Fuel Cell Technologies, Albuquerque, NM, USA) with a custom flow-field containing 14 straight parallel channels was used for each test. Fabricated MEAs were assembled with 5 cm^2 active area using the GDL combinations shown in Table 2. The thickness of the PTFE gaskets was chosen to maintain ~25 % compression considering the total thickness of GDL and catalyst layers. Also, to avoid excessive stress on the membrane, PTFE gaskets were placed proportionally to the thickness of the anode and cathode. Fuel cells were tested using a commercial test station (850e, Scribner Associates Inc., Southern Pines, NC). Electrochemical impedance spectroscopy (EIS) was measured using a BioLogic SP-240 potentiostat. First, the cell was heated to 80 °C with 500 sccm of N$_2$ at 50 % RH flowing over the anode and cathode for 2 h to hydrate the membrane and ionomer. Polarization curves and EIS were measured under different relative humidity with 1000 sccm of H$_2$ and 2000 sccm air on the anode and cathode, respectively. Tested conditions were (1) anode 50 % RH, cathode 50 % RH, 150 kPaa; (2) anode 100 % RH, cathode 100 % RH, 150 kPaa; (3) anode 100 % RH, cathode 100 % RH, 250 kPaa; and (4) anode 100 % RH, cathode 150 % RH, 150 kPaa. All cells were tested from lower humidity to higher humidity, and between each condition, 500 sccm of N$_2$ was purged on both sides for 1.5 h to equilibrate. EIS was performed at 0.5 A cm^{-2} with a current perturbation of 50 mA cm^{-2} and a frequency range from 10,000–0.1 Hz. After collecting polarization and EIS data, we measured cyclic voltammetry (CV) with a scan rate of 50 mV/s from 0.04 V to 0.95 V.

2.4. Model description

A 2D steady state, multiphase, and multiphysics model was used to study the behavior of the PEMFCs with the different asymmetric GDL configurations. The macro-homogeneous model used spatially averaged physical and transport properties for each layer. The computational domain consisted of a half channel-half land cross section of the MEA, as shown in Fig. S3. Table S1 provides an overview of the governing physics for the different phenomena accounted in the model. Table S2 highlights the different source terms in the model. The hydrogen oxidation reaction (HOR) on the anode is modeled using Butler-Volmer kinetics [34]. The current density for the ORR was calculated using an agglomerate model [35] with Tafel kinetics. The rates of water evaporation/condensation and sorption/desorption are dictated by the difference in the chemical potential between the vapor-liquid and ionomer-vapor phases,

Table 2
GDL configurations tested in this study.

	Name	Anode GDL	Cathode GDL	Difference in Gurley Number
Group 1: Lowest permeability GDL in the cathode	Cell 1	H14C10	H14C10	0
	Cell 2	H14C9	H14C10	40
	Cell 3	H14Cx653	H14C10	55
	Cell 4	H15C14	H14C10	69.4
Group 2: Highest permeability GDL in the cathode	Cell 5	H15C14	H15C14	0
	Cell 6	H14C9	H15C14	29.4
	Cell 7	H14C7	H15C14	49.4
	Cell 8	H14C10	H15C14	69.4

respectively. Water sorption/desorption between the ionomer and liquid phase only occurs if the chemical potential of the liquid phase is greater than the chemical potential of the vapor phase [36]. A detailed description of the model can be found in Refs. [34,36].

3. Results and discussion

To evaluate the performance of the different GDL configurations, polarization curves were measured under differential conditions with different relative humidity and backpressure. Under air operating conditions, Pajarito PGM-free catalyst has been shown to demonstrate an OCV lower than 0.9 V [19,20]. As shown in Fig. 1a, for the first group of cells, cells with asymmetric GDL configurations had superior performance in the mass transport region at 100 % RH compared to the baseline Cell 1, which had a symmetric GDL configuration. As the MPLs had different surface morphology (Fig. S1), we also report the HFR-corrected data in Fig. S4a to correct for any possible performance variation due to the contact resistance or hydration state of the membrane. All cells showed similar performance at low current densities, implying that increasing the permeability of the anode GDL does not have any impact on kinetics or ohmic resistance. Cyclic voltammograms showed similar double layer capacitance (Fig. S4b), confirming that all MEAs had similar catalyst loading. EIS at 0.5 A cm^{-2} revealed that the cell impedance decreased monotonically as the anode GDL permeability increased (Fig. 1b). As all the MEAs had similar catalyst loading and similar kinetic performance, the decrease in impedance is attributed to reduction in the mass transport resistance as the permeability difference increased.

For further understanding of mass transport, we tested the performance under three more conditions.

- Dry condition (anode 50 % RH, cathode 50 % RH, 150 kPaa);
- Wet condition with high pressure (anode 100 % RH, cathode 100 % RH, 250 kPaa)
- Flooded condition (anode 100 % RH, cathode 150 % RH, 150 kPaa).

Polarization curves and EIS measured in these different conditions are shown in Fig. S5. Under 50 % RH, all four cells had similar performance (Fig. 2a, Fig. S5a). However, upon increasing the humidity to 100 % RH, the cell with the largest difference in GDL permeability (Cell 4) showed a performance increase of 100 mV at 1 A cm^{-2} compared to the cell with symmetric GDL configuration (Cell 1) (Fig. 2b). Increasing the total operating pressure to 250 kPa caused significant performance increases for the cells with asymmetric GDL configurations, while the MEA with symmetric GDL configuration (Cell 1) showed barely any performance increase (Fig. 2c). These results imply that the asymmetric GDL configuration, with lowest permeability GDL in the cathode, provided enhanced water management under highly saturated conditions. This conclusion is further supported by the large difference in performance under oversaturated condition (150 % RH on the cathode), where the baseline Cell 1 was not able to achieve 1 A cm^{-2}, whereas Cell 4 reached 200 mV at 1 A cm^{-2}. Although the asymmetric GDL configurations provided similar performance to the symmetric GDL configuration under dry operating conditions, under wet or flooded conditions, anode GDLs with higher permeability provided improved water management, increasing mass transport and improving performance at high current density. Improved transport of oxygen is due to lower water saturation caused by back diffusion of water which is further explained in the modeling section.

Polarization performance and EIS of the second group of cells, in which the highest permeability GDL was used on the cathode, is shown in Fig. 3. In contrast with the first group of cells, the second group showed minimal differences in polarization performance (Fig. 3a and Fig. S6a) or EIS (Fig. 3b) under fully humidified conditions. Fuel cell performance at 1 A cm^{-2} for dry, wet, and flooded conditions (Fig. S7) showed no significant change with anode permeability, in agreement with observed behavior in the full polarization curves and EIS plots (Fig. S8).

A computational continuum model was used to provide further understanding of water management in the asymmetric GDL configuration. The numerical model requires the capillary pressure-saturation relationships for the PGM free catalyst layers to accurately describe the two-phase transport in these layers. Since water retention curves for PGM free electrodes have not been characterized, the average saturation in the cathode CL was fit to numerically reproduce the experimental results.
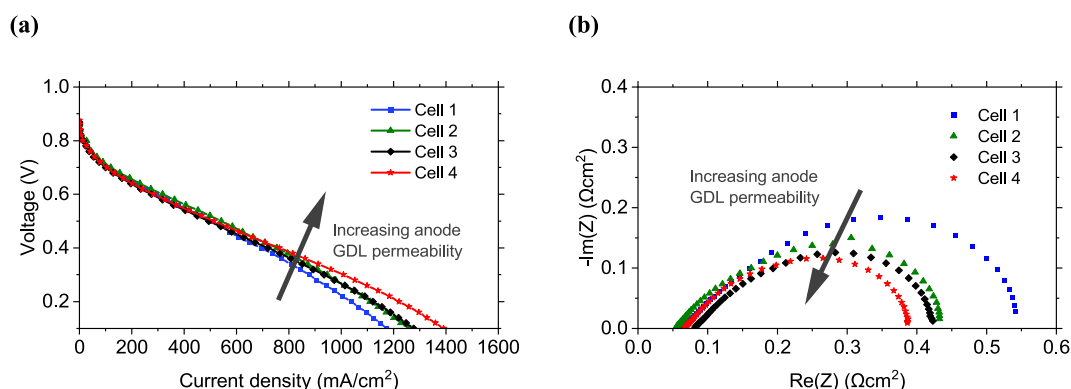

Fig. 1. Comparison of cell performance of the first group of cells at 100 % RH. (a) Cell polarization; (b) EIS at 0.5 A cm^{-2}. Conditions: 80 °C cell temperature, 1000/2000 sccm H$_2$/air, 150 kPaa.
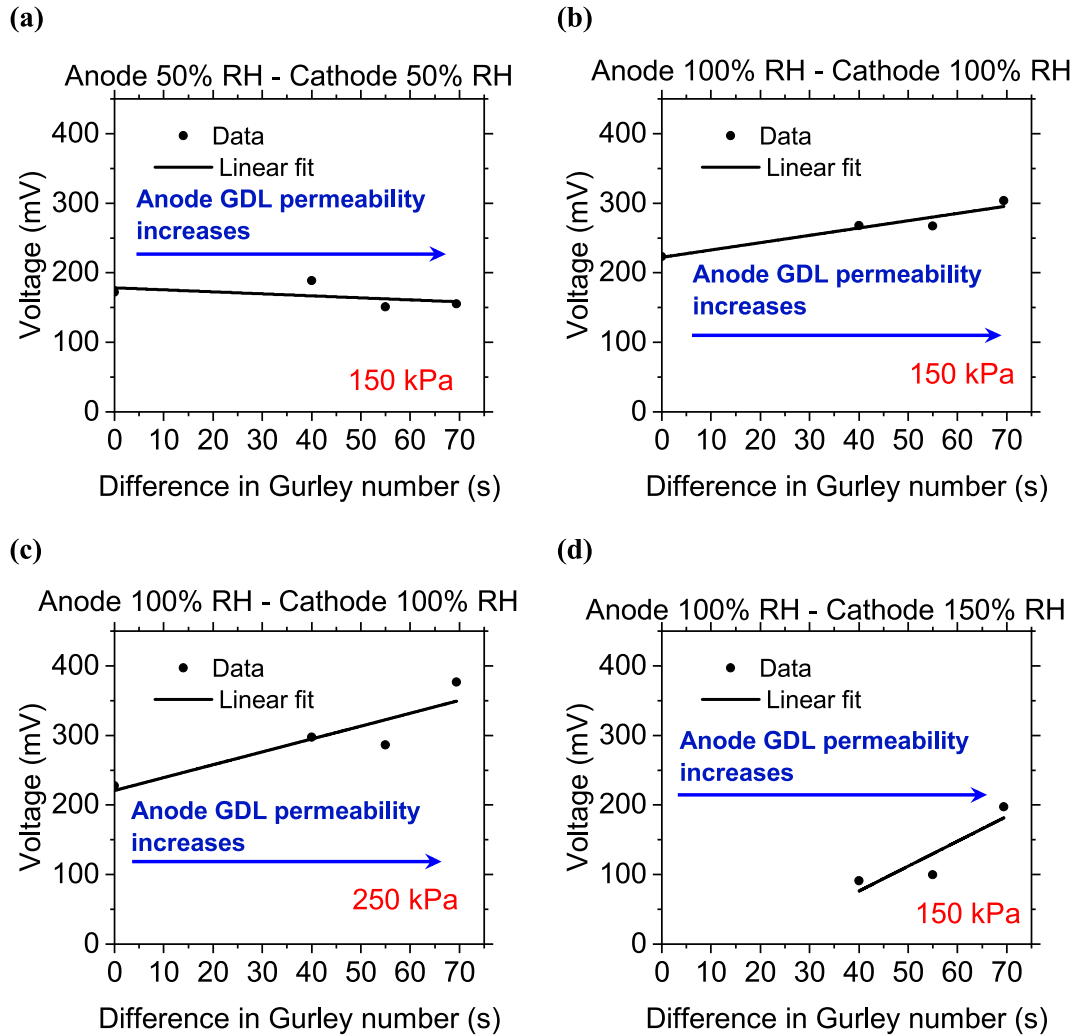
(a)

(b)

(c)

(d)

Fig. 2. Voltage at 1 A cm^{-2} with respect to the difference in Gurley number between anode and cathode GDL for the first group of cells. (a) Anode 50 % RH, cathode 50 % RH, 150 kPaa; (b) anode 100 % RH, cathode 100 % RH, 150 kPaa; (c) anode 100 % RH, cathode 100 % RH, 250 kPaa; (d) anode 100 % RH, cathode 150 % RH, 150 kPaa. Severe flooding of the cell with symmetric GDL configuration under 150 % RH prevented the current from reaching 1 A cm^{-2}. Cell temperature: 80 °C; flow rate H$_2$/air: 1000/2000 sccm.
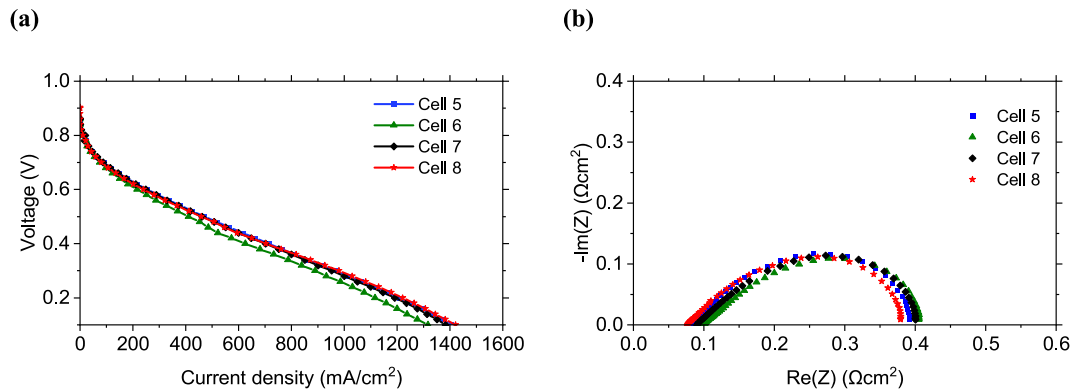
(a)

(b)

Fig. 3. Comparison of cell performance of the second group of cells at 100 % RH. a) Cell polarization; (b) EIS. Conditions: 80 °C cell temperature, 1000/2000 sccm H$_2$/air, 150 kPaa.

The model results show good agreement with the experimental polarization curves, as shown in Fig. 4 for both groups of cells. For the first group of cells with low permeability GDL on the cathode, the model predicts an improvement in performance due to a reduction in the average cathode CL saturation from 0.57 for Cell 1, 0.5 for Cells 2 and 3, and 0.44 for Cell 4. The average capillary pressure (defined as the difference between the liquid and gas pressure) in the cathode CL for Cell 1 is 20 Pa higher than Cell 4 at 1 A cm^{-2}. The relatively small difference in capillary pressure resulting in a 13 % saturation change is indicative of a sharp gradient in the water retention curve. For the second group of cells with high permeability GDL on the cathode, the average cathode CL saturation remained the same at 0.44 for all the cells. The voltage loss due to mass transport, evaluated using the power-loss post processing method as described by Pant et al. [37], is shown in Fig. 5. For the cells with the lowest permeability GDL in the cathode (first group), the mass transport losses decreased with increasing anode permeability due to a reduction in the cathode CL saturation. The difference in losses was higher at 1 A cm^{-2} compared to 0.5 A cm^{-2}, consistent with the observed fuel cell performance (Fig. 1a). For the cells with the highest permeability GDL in the cathode (second group), the voltage loss due to mass transport was similar, suggesting improved mass transport in the cathode irrespective of the anode GDL.

As noted above, a comparison of cells in the first group (low permeable cathode) and second group (high cathode GDL permeability) reveals a relatively weak dependence on asymmetric permeability for the second group, in contrast with the strong dependence observed in the first group. While the use of highly permeable GDLs on both anode and cathode (symmetric configuration) could in principle provide faster mass transport, examination of the most asymmetric configuration from the first group (Cell 4) in comparison with a symmetric combination of highly permeable GDLs from the second group (Cell 5) reveals some advantage for the asymmetric case (Fig. 6). Specifically, this comparison shows that a highly asymmetric GDL combination (Cell 4) can provide slightly higher performance than a symmetric combination of highly permeable GDLs (Cell 5) under the flooded operation condition, although the difference was minimal under non-flooded operation. The improved performance under the flooded condition achieved with a lower permeable GDL on the cathode may be ascribed to increased back-diffusion of water from cathode to anode and better contact between catalyst layer and GDL. This finding remains relevant to practical applications, as localized flooding can occur even under nominally low humidity operating conditions in commercial fuel cell stacks due to non-uniform water generation and distribution across the membrane electrode assembly.

The performance of PGM-free catalysts displays variability between batches. In this study, all the MEAs mentioned in the manuscript were assembled using catalyst from a single batch. While the limited batch size did not allow us to conduct repeated experiments with identical GDL configurations, we did collect multiple datasets using catalysts from different batches and various GDLs. These additional experiments consistently validated the advantage of employing an asymmetric GDL configuration that incorporates highly permeable GDLs in the anode as exemplified in Fig. S9.

Lastly, as water back diffusion is one of the key drivers for the performance improvement found in this study, use of pressure differentials or thinner membrane could also provide a means of providing enhanced water management. Each approach conveys advantages and disadvantages. While use of pressure differentials could provide flexibility for adjusting water management in real time, it would result in increased system complexity, and would also place more constraints on the required compressor output and turndown ratio. Use of thinner membranes conveys advantages in simultaneously increasing water back-diffusion and reducing membrane Ohmic losses, but it also reduces membrane durability, increases vulnerability to manufacturing defects, and increases hydrogen crossover. A full analysis of the pros and cons of each method is beyond the scope of this report, but we note in passing that asymmetric GDL design and selection provides an additional tool that can be used either alone or in combination with differential pressure and thinner membranes to provide enhance water management.

4. Conclusion

This work investigated the effect of different GDL configurations on the anode and cathode with PGM-free electrodes. Under dry conditions, GDL configuration was found to have minimal impact on performance, but under wet and flooded conditions, maximum
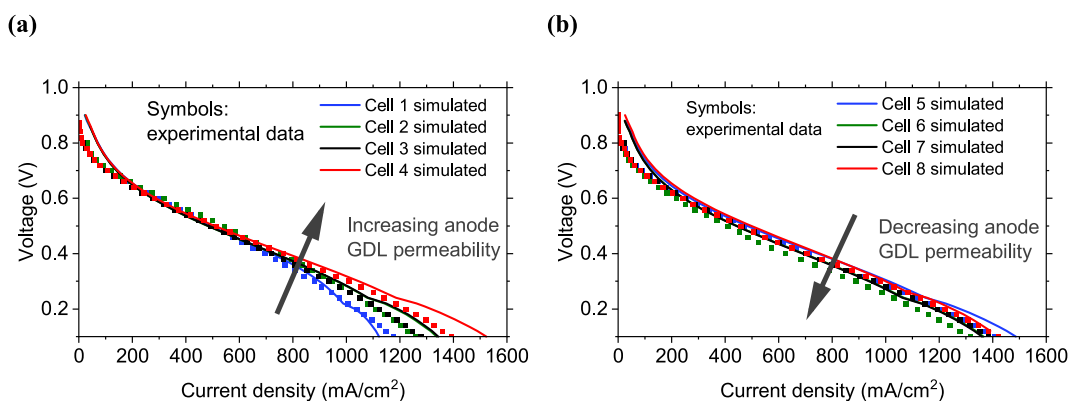

Fig. 4. Comparison of simulated and experimental cell performance for (a) first group of cells and (b) second group of cells. 80 °C cell temperature, 1000/2000 sccm H_2/air, 150 kPaa.
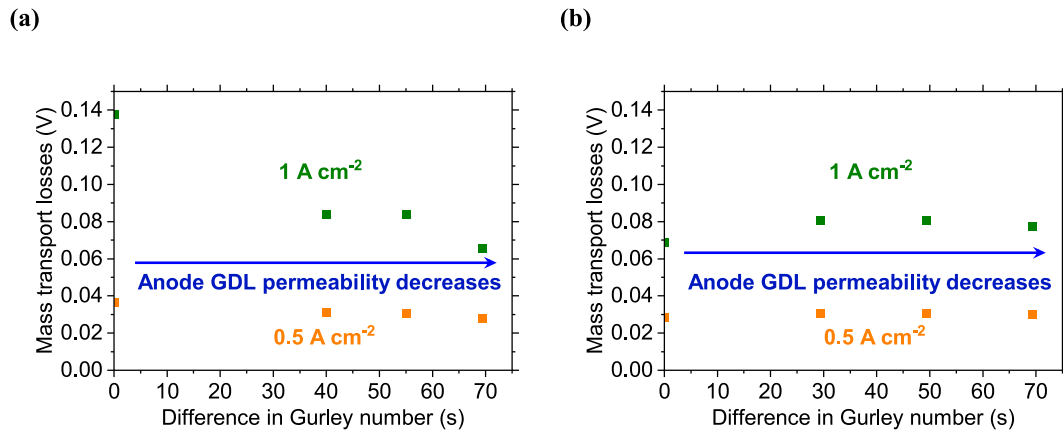
(a)   **(b)**

Fig. 5. Mass transport voltage loss at 0.5 A cm^{-2} and 1 A cm^{-2} for (a) first group of cells (lowest permeability GDL on cathode), and (b) second group of cells (highest permeability GDL on cathode).

(a)   **(b)**
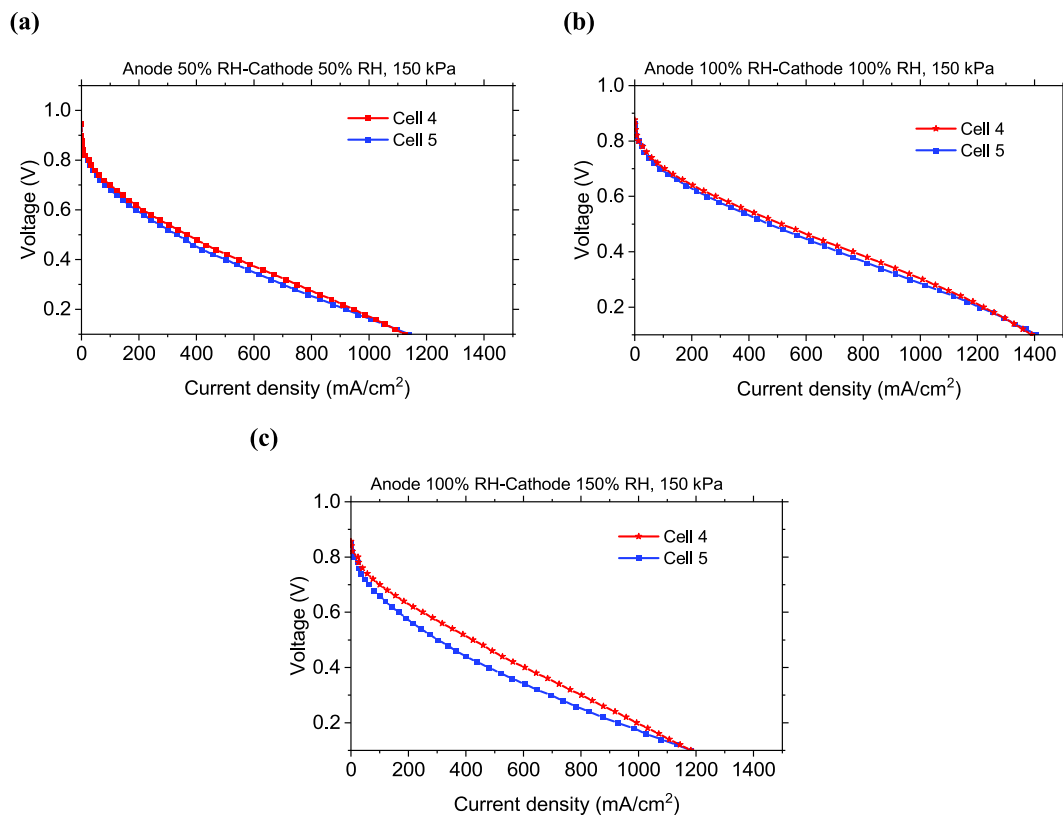
(c)

Fig. 6. Comparison between Cell 4 (anode H15C14 and cathode H14C10) and Cell 5 (anode H15C14 and cathode H15C14) at (a) anode 50 % RH-cathode 50 % RH, (b) anode 100 % RH-cathode 100 % RH, (c) anode 100 % RH-cathode 150 % RH. Cell temperature: 80 °C, flow rate H$_2$/air: 1000/2000 sccm, back pressure: 150 kPaa.

performance was achieved with a low permeability GDL on the cathode and a high permeability GDL on the anode. Computational modeling revealed that this improvement was mainly due to lower liquid water saturation in the cathode and overall better water management. When using a low permeability GDL on the cathode, the fuel cell performance showed a direct correlation to the difference in permeability between anode and cathode GDLs. When using a high permeability GDL on the cathode, the permeability of the anode GDL had minimal effect on performance. Overall, this study demonstrates that improved water management can be achieved by tuning the permeability of anode and cathode GDLs.

CRediT authorship contribution statement

Tanvir Alam Arman: Conceptualization, Investigation, Writing – original draft. **Siddharth Komini Babu:** Conceptualization, Supervision, Writing – original draft. **Mayank Sabharwal:** Investigation, Writing – original draft. **Adam Z. Weber:** Supervision, Writing – review & editing. **Ugur Pasaogullari:** Supervision, Writing – review & editing. **Jacob S. Spendelow:** Conceptualization, Funding acquisition, Supervision, Writing – review & editing.

Declaration of competing interest

The authors declare that they have no known competing financial interests or personal relationships that could have appeared to influence the work reported in this paper.

Acknowledgement

Appendix A. Supplementary data

Supplementary data to this article can be found online at https://doi.org/10.1016/j.heliyon.2024.e37222.

References

[1] D. Papageorgopoulos, Fuel cells R&D overview - 2018 annual merit review and peer evaluation meeting. https://doi.org/10.1007/s11187-015-9640-6, 2018.
[2] J. Li, M.T. Sougrati, A. Zitolo, J.M. Ablett, I.C. Oğuz, T. Mineva, I. Matanovic, P. Atanassov, Y. Huang, I. Zenyuk, A. Di Cicco, K. Kumar, L. Dubau, F. Maillard, G. Dražić, F. Jaouen, Identification of durable and non-durable FeNx sites in Fe–N–C materials for proton exchange membrane fuel cells, Nat. Catal. 4 (2021) 10–19, https://doi.org/10.1038/s41929-020-00545-2.
[3] H. Zhang, H.T. Chung, D.A. Cullen, S. Wagner, U.I. Kramm, K.L. More, P. Zelenay, G. Wu, High-performance fuel cell cathodes exclusively containing atomically dispersed iron active sites, Energy Environ. Sci. 12 (2019) 2548–2558, https://doi.org/10.1039/c9ee00877b.
[4] L. Jiao, J. Li, L.L.R. Richard, Q. Sun, T. Stracensky, E. Liu, M.T. Sougrati, Z. Zhao, F. Yang, S. Zhong, H. Xu, S. Mukerjee, Y. Huang, D.A. Cullen, J.H. Park, M. Ferrandon, D.J. Myers, F. Jaouen, Q. Jia, Chemical vapour deposition of Fe–N–C oxygen reduction catalysts with full utilization of dense Fe–N4 sites, Nat. Mater. 20 (2021) 1385–1391, https://doi.org/10.1038/s41563-021-01030-2.
[5] U. Martinez, S. Komini Babu, E.F. Holby, H.T. Chung, X. Yin, P. Zelenay, Progress in the development of Fe-based PGM-free electrocatalysts for the oxygen reduction reaction, Adv. Mater. 31 (2019), https://doi.org/10.1002/adma.201806545.
[6] J. Xie, 2021 Annual Merit Reveiw and Peer Evaluation Meeting, 2021.
[7] S. Litster, Advanced PGM-free cathode engineering for high power density and durability, in: 2020 Annual Merit Review Proceedings, 2020. https://www.hydrogen.energy.gov/pdfs/review20/fc171_litster_2020_o.pdf.
[8] A. Uddin, L. Dunsmore, H. Zhang, L. Hu, G. Wu, S. Litster, High power density platinum group metal-free cathodes for polymer electrolyte fuel cells, ACS Appl. Mater. Interfaces 12 (2020) 2216–2224, https://doi.org/10.1021/acsami.9b13945.
[9] H.T. Chung, D.A. Cullen, D. Higgins, B.T. Sneed, E.F. Holby, K.L. More, P. Zelenay, Direct atomic-level insight into the active sites of a high-performance PGM-free ORR catalyst, Science 357 (2017) 479–484, https://doi.org/10.1126/science.aan2255, 1979.
[10] H. Zhang, S. Hwang, M. Wang, Z. Feng, S. Karakalos, L. Luo, Z. Qiao, X. Xie, C. Wang, D. Su, Y. Shao, G. Wu, Single atomic iron catalysts for oxygen reduction in acidic media: particle size control and thermal activation, J. Appl. Comput. Sci. (2017), https://doi.org/10.1021/jacs.7b06514.
[11] H. Zhang, H.T. Chung, D.A. Cullen, S. Wagner, U.I. Kramm, K.L. More, P. Zelenay, G. Wu, High-performance fuel cell cathodes exclusively containing atomically dispersed iron active sites, Energy Environ. Sci. 12 (2019) 2548–2558, https://doi.org/10.1039/c9ee00877b.
[12] Y. He, G. Wu, PGM-free oxygen-reduction catalyst development for proton-exchange membrane fuel cells: challenges, solutions, and promises, Acc. Mater. Res. 3 (2022) 224–236, https://doi.org/10.1021/accountsmr.1c00226.
[13] D. Myers, P. Zelenay, ElectroCat (electrocatalysis consortium), in: 2018 Annual Merit Review and Peer Evaluation Meeting, 2019, pp. 1–54.
[14] S. Komini Babu, D. Spernjak, R. Mukundan, D.S. Hussey, D.L. Jacobson, H.T. Chung, G. Wu, A.J. Steinbach, S. Litster, R.L. Borup, P. Zelenay, Understanding water management in platinum group metal-free electrodes using neutron imaging, J. Power Sources 472 (2020) 228442, https://doi.org/10.1016/j.jpowsour.2020.228442.
[15] S. Komini Babu, H.T. Chung, P. Zelenay, S. Litster, Resolving electrode morphology's impact on platinum group metal-free cathode performance using nano-CT of 3D hierarchical pore and ionomer distribution, ACS Appl. Mater. Interfaces 8 (2016) 32764–32777, https://doi.org/10.1021/acsami.6b08844.
[16] D. Banham, T. Kishimoto, Y. Zhou, T. Sato, K. Bai, J.I. Ozaki, Y. Imashiro, S. Ye, Critical advancements in achieving high power and stable nonprecious metal catalyst-based MEAs for real-world proton exchange membrane fuel cell applications, Sci. Adv. 4 (2018), https://doi.org/10.1126/sciadv.aar7180.
[17] A. Uddin, L. Dunsmore, H. Zhang, L. Hu, G. Wu, S. Litster, High power density platinum group metal-free cathodes for polymer electrolyte fuel cells, ACS Appl. Mater. Interfaces 12 (2020) 2216–2224, https://doi.org/10.1021/acsami.9b13945.
[18] H. Wang, L. Osmieri, H. Yu, M.J. Zachman, J.H. Park, N.N. Kariuki, F.C. Cetinbas, S. Khandavalli, S. Mauger, D.J. Myers, D.A. Cullen, K.C. Neyerlin, Elucidating the impact of the ionomer equivalent weight on a platinum group metal-free PEMFC cathode via oxygen limiting current, SusMat 3 (2023) 72–90, https://doi.org/10.1002/sus2.106.
[19] G. Wang, L. Osmieri, A.G. Star, J. Pfeilsticker, K.C. Neyerlin, Elucidating the role of ionomer in the performance of platinum group metal-free catalyst layer via in situ electrochemical diagnostics, J. Electrochem. Soc. 167 (2020) 044519, https://doi.org/10.1149/1945-7111/ab7aa1.
[20] L. Osmieri, G. Wang, F.C. Cetinbas, S. Khandavalli, J. Park, S. Medina, S.A. Mauger, M. Ulsh, S. Pylypenko, D.J. Myers, K.C. Neyerlin, Utilizing ink composition to tune bulk-electrode gas transport, performance, and operational robustness for a Fe–N–C catalyst in polymer electrolyte fuel cell, Nano Energy 75 (2020), https://doi.org/10.1016/j.nanoen.2020.104943.
[21] I.V. Zenyuk, D.Y. Parkinson, L.G. Connolly, A.Z. Weber, Gas-diffusion-layer structural properties under compression via X-ray tomography, J. Power Sources 328 (2016) 364–376, https://doi:10.1016/j.jpowsour.2016.08.020.

[22] A. El-Kharouf, T.J. Mason, D.J.L. Brett, B.G. Pollet, Ex-situ characterisation of gas diffusion layers for proton exchange membrane fuel cells, J. Power Sources 218 (2012) 393–404. https://doi:10.1016/j.jpowsour.2012.06.099.

[23] M. Sarker, A. Rahman, F. Mojica, S. Mehrazi, W.J.M. Kort-Kamp, P.Y.A. Chuang, Experimental and computational study of the microporous layer and hydrophobic treatment in the gas diffusion layer of a proton exchange membrane fuel cell, J. Power Sources 509 (2021) 230–350. https://doi:10.1016/j.jpowsour.2021.230350.

[24] R. Schweiss, Benefits of membrane electrode assemblies with asymmetrical GDL configurations for PEM fuel cells, Fuel Cell. 16 (2016) 100–106, https://doi.org/10.1002/fuce.201500133.

[25] M.P. Manahan, J.T. Clement, A.K. Srouji, S.W. Brown, T. Reutzel, M.M. Mench, Laser modified fuel cell diffusion media: engineering enhanced performance via localized water redistribution, J. Electrochem. Soc. 161 (2014) F1061–F1069, https://doi.org/10.1149/2.0591410jes.

[26] J.H. Chun, K.T. Park, D.H. Jo, J.Y. Lee, S.G. Kim, S.H. Park, E.S. Lee, J.Y. Jyoung, S.H. Kim, Development of a novel hydrophobic/hydrophilic double micro porous layer for use in a cathode gas diffusion layer in PEMFC, Int. J. Hydrogen Energy 36 (2011) 8422–8428, https://doi.org/10.1016/j.ijhydene.2011.04.038.

[27] T. Kitahara, T. KonomiI, H. Nakajima, M. Murata, Effects of design parameters in paper type gas diffusion layer on the performance of polymer electrolyte fuel cells (measures to prevent flooding and drying-up), J. Environ. Eng. 4 (2009) 338–345, https://doi.org/10.1299/jee.4.338.

[28] L. Holzer, O. Pecho, J. Schumacher, P. Marmet, F.N. Büchi, A. Lamibrac, B. Münch, Microstructure-property relationships in a gas diffusion layer (GDL) for Polymer Electrolyte Fuel Cells, Part II: pressure-induced water injection and liquid permeability, Electrochim. Acta 241 (2017) 414–432, https://doi.org/10.1016/j.electacta.2017.04.141.

[29] R. Schweiss, M. Steeb, P.M. Wilde, T. Schubert, Enhancement of proton exchange membrane fuel cell performance by doping microporous layers of gas diffusion layers with multiwall carbon nanotubes, J. Power Sources 220 (2012) 79–83, https://doi.org/10.1016/j.jpowsour.2012.07.078.

[30] T. Kitahara, H. Nakajima, K. Okamura, Gas diffusion layers coated with a microporous layer containing hydrophilic carbon nanotubes for performance enhancement of polymer electrolyte fuel cells under both low and high humidity conditions, J. Power Sources 283 (2015) 115–124, https://doi.org/10.1016/j.jpowsour.2015.02.115.

[31] L. Dunsmore, A. Uddin, H. Zhang, G. Wu, S. Litster, Non-planar platinum group metal-free fuel cell cathodes for enhanced oxygen transport and water rejection, J. Power Sources 506 (2021) 230188, https://doi.org/10.1016/j.jpowsour.2021.230188.

[32] Freudenberg GDL technical data sheet, n.d. https://www.fuelcellstore.com/spec-sheets/freudenberg-gdl-technical-data.pdf (accessed November 7, 2022.

[33] Freudenberg GDL technical data sheet-H15C14, (n.d.). https://www.fuelcellstore.com/spec-sheets/freudenberg-gdl-technical-sheet-h15c14.pdf (accessed November 7, 2022).

[34] I.v. Zenyuk, P.K. Das, A.Z. Weber, Understanding impacts of catalyst-layer thickness on fuel-cell performance via mathematical modeling, J. Electrochem. Soc. 163 (2016) F691–F703, https://doi.org/10.1149/2.1161607jes.

[35] M. Secanell, K. Karan, A. Suleman, N. Djilali, Multi-variable optimization of PEMFC cathodes using an agglomerate model, Electrochim. Acta 52 (2007) 6318–6337, https://doi.org/10.1016/j.electacta.2007.04.028.

[36] L.M. Pant, M.R. Gerhardt, N. Macauley, R. Mukundan, R.L. Borup, A.Z. Weber, Along-the-channel modeling and analysis of PEFCs at low stoichiometry: Development of a 1+2D model, Electrochim. Acta 326 (2019) 134963, https://doi.org/10.1016/j.electacta.2019.134963.

[37] M.R. Gerhardt, L.M. Pant, J.C. Bui, A.R. Crothers, V.M. Ehlinger, J.C. Fornaciari, J. Liu, A.Z. Weber, Method—practices and pitfalls in voltage breakdown analysis of electrochemical energy-conversion systems, J. Electrochem. Soc. 168 (2021) 074503, https://doi.org/10.1149/1945-7111/abf061.